INSTITUTE OF PHYSICS PUBLISHING JOURNAL OF PHYSICS: CONDENSED MATTER

J. Phys.: Condens. Matter **16** (2004) 809–819 PII: S0953-8984(04)68683-8

Raman and infrared-active phonons in hexagonal $HoMnO_3$ single crystals: magnetic ordering effects

A P Litvinchuk[1,4], M N Iliev[1], V N Popov[2] and M M Gospodinov[3]

[1] Texas Center for Superconductivity and Advanced Materials and Department of Physics, University of Houston, Houston, TX 77204-5002, USA
[2] Faculty of Physics, University of Sofia, 1164 Sofia, Bulgaria
[3] Institute of Solid State Physics, Bulgarian Academy of Sciences, 1184 Sofia, Bulgaria

E-mail: Alexander.Litvinchuk@mail.uh.edu

Received 8 September 2003, in final form 27 November 2003
Published 30 January 2004
Online at stacks.iop.org/JPhysCM/16/809 (DOI: 10.1088/0953-8984/16/6/011)

Abstract

Polarized first- and second-order Raman scattering and infrared reflection spectra of hexagonal $HoMnO_3$ single crystals in the temperature range 10–300 K are reported. Based on the symmetry analysis and comparison with the results of lattice dynamics calculations the observed lines are assigned to the lattice eigenmodes. The magnetic ordering of Mn ions, which occurs below $T_N = 76$ K, is shown to affect Raman- and infrared-active phonons, which modulate Mn–O–Mn bonds and, consequently, the Mn–Mn exchange interaction.

1. Introduction

The hexagonal $RMnO_3$ (R = Ho, Er, Tm, Yb, Lu, Y; space group $P6_3cm$ (C_{6v}^3), $Z = 6$) compounds belong to the class of ferroelectromagnetic materials characterized by the coexistence of antiferromagnetic (AFM) and ferroelectric (FE) orders [1, 2]. The FE and AFM transitions are well separated with Curie and Néel temperatures being $T_C > 800$ K and $T_N \approx 76$ K, and only weak coupling of the two respective order parameters is expected. Such coupling does exist in $RMnO_3$ materials. For $YMnO_3$, for instance, anomalies in the dielectric constant and loss tangent near T_N [3] and an additional antiferromagnetic contribution to the non-linear optical polarizability below T_N [4–6] were found experimentally. Furthermore, a number of magnetic transitions below T_N were established for $HoMnO_3$ due to both Mn in-xy-plane and Ho z-axis ordering [7, 8]. The Raman scattering is determined by non-linear terms of polarizability, which may be affected by AFM–FE and/or spin-phonon couplings. In the case of strong couplings the Raman spectra should exhibit anomalies at magnetic transition temperatures. Anomalous Raman scattering due to two-magnon processes was

[4] Author to whom any correspondence should be addressed.

recently reported for $YMnO_3$ [9], but not confirmed in more recent studies [10, 11]. All theses facts give a motivation for a more thorough study of lattice vibrations of hexagonal manganites as a function of temperature.

In this paper we report the polarized Raman and infrared reflection spectra of $HoMnO_3$ single crystals in a broad temperature range. Pronounced phonon anomalies, that are related to spin-phonon or AFM–FE couplings, are observed experimentally. A comparison to the mode frequencies predicted by lattice dynamics calculations allowed assignment of the Raman and infrared lines to definite phonon modes or two-phonon Raman scattering processes. No evidence for two-magnon scattering was found in the low temperature antiferromagnetic phase.

2. Samples and experimental details

Pure polycrystalline hexagonal $HoMnO_3$ was synthesized by a solid-state reaction of stoichiometric amounts of Ho_2O_3 (99.99%) and MnO_2 (99.99%), and further annealed for 24 h at 1120 °C in an oxygen atmosphere. $HoMnO_3$ single crystals were grown by a high temperature solution growth method using $PbF_2/PbO/B_2O_3$ flux (PbF_2:PbO:B_2O_3 = 0.8:0.195:0.005). The flux was mixed with $HoMnO_3$ powder in a 7:1 ratio and annealed in a platinum crucible at 1250 °C for 48 h in oxygen. After that the temperature was decreased down to 1000 °C at a rate of 0.5 °C h^{-1}. The flux was decanted and well-shaped hexagonal plate-like crystals of typical size $3 \times 5 \times 0.2$ mm^3 removed from the bottom of the crucible.

The Raman spectra were measured under a microscope using a HR640 spectrometer equipped with a liquid-nitrogen-cooled CCD detector. The 514.5 and 632.8 nm lines of Ar^+ and He–Ne lasers were used for excitation. The infrared reflectance was measured with a Bomem DA8 Fourier-transform interferometer equipped with a near-normal incidence reflectance stage and a liquid-helium-cooled bolometer. The real and imaginary parts of the dielectric function, $\epsilon_1(\omega)$ and $\epsilon_2(\omega)$, were obtained through Kramers–Kronig analysis.

3. Results and discussion

3.1. Room temperature data and lattice dynamics calculations

The elementary cell of hexagonal $RMnO_3$ (space group $P6_3cm$, C_{6v}^3, $Z = 6$) is displayed in figure 1. The group-theoretical analysis [12] shows that long-wavelengths zone-centre (Γ-point) phonons are distributed among irreducible representations of the C_{6v} point group as follows:

$$\Gamma_{tot} = 10A_1 + 5A_2 + 10B_1 + 5B_2 + 15E_1 + 15E_2.$$

Of them acoustic, Raman-active and infrared-active phonons are, respectively,

$$\Gamma_{ac} = A_1 + E_1;$$
$$\Gamma_R = 9A_1 + 14E_1 + 15E_2;$$
$$\Gamma_{IR} = 9A_1 + 14E_1.$$

The optical modes of A_2, B_1 and B_2 symmetries are silent. Depending on the scattering configuration one can activate either longitudinal optical (LO) A_1 modes, when the phonon propagation direction coincides with the direction of ion displacements ($z(xx)\bar{z}$ polarization), or transverse (TO) modes ($y(xx)\bar{y}$ and $y(zz)\bar{y}$ configurations). Non-polar E_2 vibrations are allowed in $z(xy)\bar{z}$ polarization, while E_1 are Raman-active in $y(zx)\bar{y}$ polarization. In the latter case experimentally observed E_1 modes have transverse character.

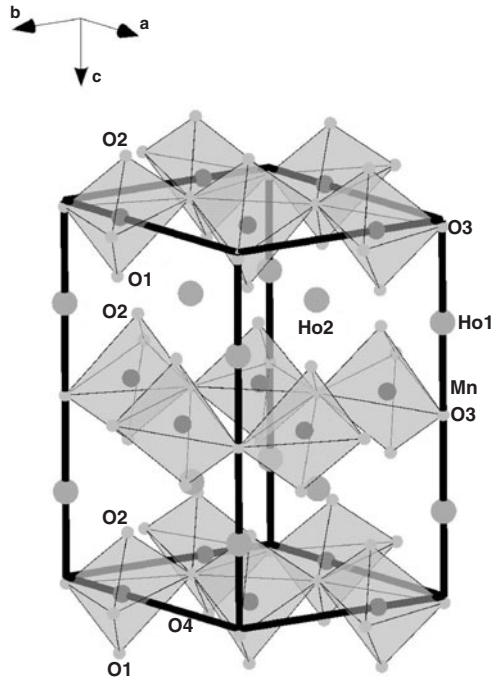

Figure 1. Crystallographic structure of hexagonal $HoMnO_3$ (after parameters of [8]).

As the crystals are non-centrosymmetric, the modes of A_1 and E_1 symmetry are also infrared-active and modulate the dipole moment along the z axis and within the xy plane, respectively. Optical reflection spectra from the large xy plane surfaces correspond to the case when incident and reflected light propagate along the z axis and are polarized in the xy plane ($\vec{E} \perp z$). As a consequence, E_1 but not A_1 phonons are accessible in this experimental configuration.

Figure 2 shows the polarized Raman spectra of $HoMnO_3$ at room temperature obtained with two different excitation wavelengths. The most intense spectral feature in both cases is the high-frequency line at 685 cm^{-1}, which corresponds to the apical oxygen (O1, O2) stretching vibration along the z axis around the Mn ions. The relative line intensities depend strongly on the laser excitation energy. In particular, the line at 136 cm^{-1} is not observed in the spectra taken with 1.96 eV ($\lambda_{exc} = 632.8$ nm) excitation. Another noticeable feature is the variation with λ_{exc} of the $(xx)/(zz)$ relative intensity for the 685 cm^{-1} mode: for $\lambda_{exc} = 514.5$ nm the line intensity in (zz) polarization is stronger by a factor of 10 compared to (xx), while these lines are of similar intensity with $\lambda_{exc} = 632.8$ nm. These facts indicate strong resonant behaviour of the Raman spectra, which occurs when incident or scattered light energies are in resonance with a real electronic transition in the material under investigation. Indeed, for $HoMnO_3$ a polarized ($\vec{E} \perp z$) on-side Mn d–d transition near 1.7 eV dominates the absorption spectrum in the visible spectral range [13], similar to the case of $LuMnO_3$ [14].

In figure 3 reflection spectra are shown along with the imaginary part of the dielectric function $\epsilon_2(\omega)$ and the loss function $\mathrm{Im}(-1/\epsilon)$, the maxima of which yield the position of the transverse and longitudinal excitations, respectively. The experimental and theoretical values of the Γ-point mode frequencies are summarized in tables 1 and 2.

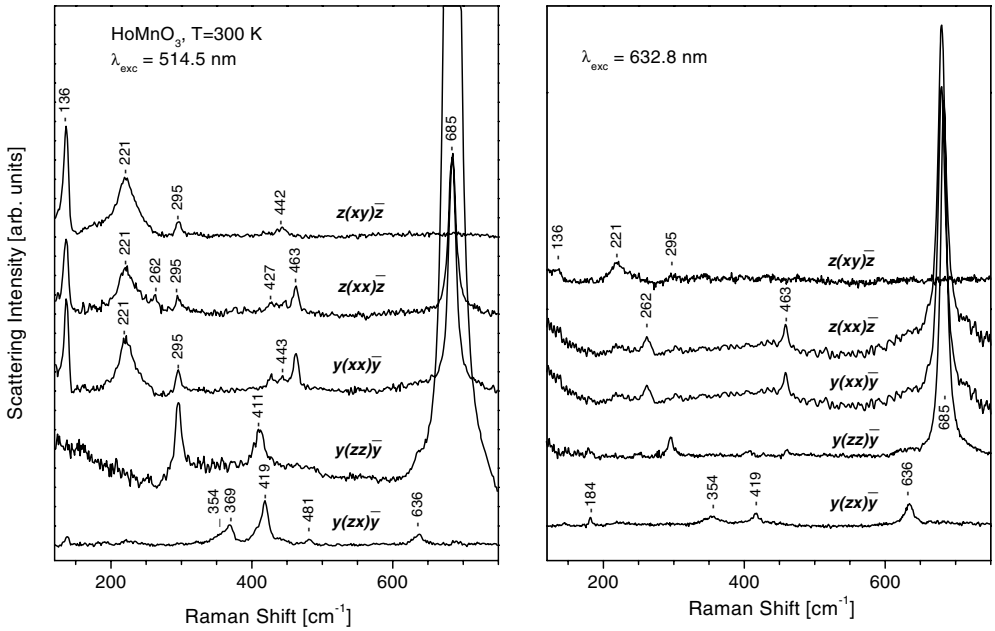

Figure 2. Room temperature polarized Raman scattering spectra of hexagonal $HoMnO_3$ crystals for excitation wavelengths $\lambda_{exc} = 514.5$ nm (left panel) and 632.8 nm (right panel). According to the selection rules, the spectra correspond to the following symmetries (from top to bottom): E_2, $A_1(LO) + E_2$, $A_1(TO) + E_2$, $A_1(TO)$ and $E_1(TO)$.

The lattice dynamics calculations were carried out within a shell model [15]. Lattice parameters and the atomic position of hexagonal $HoMnO_3$ were adopted from [8]. The interionic interactions are described by Coulomb potentials and short-range potentials of the Born–Mayer type $a\exp(-br)$, where r is the interionic separation. The O–O short-range potential is chosen in the Born–Mayer–Buckingham form $a\exp(-br) - c/r^6$. The ionic polarizability is modelled by representing each ion as a charged point core and a spherical massless shell with charge Y. The core and the shell are coupled through a spring with a force constant k. The ionic charge Z, the shell charge Y and the ionic polarizability $\alpha = Y^2/k$, along with the parameters of the short-range potentials a, b and c, are considered as independent parameters of the model. These parameters are derived by fitting experimental data on elastic properties and phonon frequencies of simpler perovskite-like compounds [12, 15]. The values of these parameters for $HoMnO_3$ are listed in table 3.

Similar to the case of the isostructural $YMnO_3$ compound [12], more than half of the expected phonons of $HoMnO_3$ are observed experimentally and assigned to definite lattice modes. Comparison of mode frequencies of $YMnO_3$ (table 4 of [12]) and $HoMnO_3$ (tables 1 and 2) shows their close similarity. In the case of E_1-symmetry modes the experimentally observed TO frequencies of $HoMnO_3$, as obtained from the Raman and infrared spectra, are in very good agreement (table 2).

3.2. Temperature-dependent Raman and infrared spectra

As far as the temperature dependence of Raman-active phonon parameters is concerned, most of the phonons exhibit standard anharmonicity-related frequency hardening and linewidth narrowing upon decreasing temperature, proving the absence of any major structural transitions

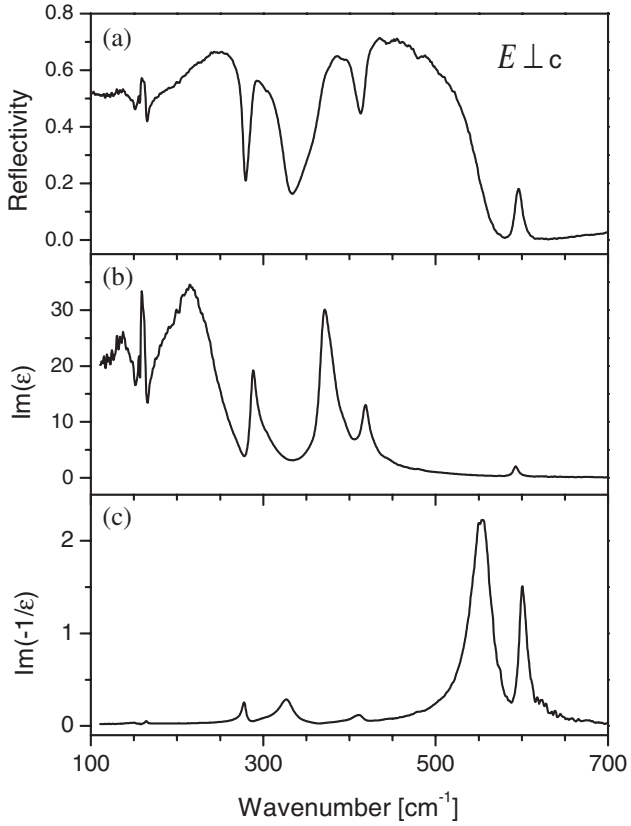

Figure 3. Spectral dependence of reflectivity (a), Im(ϵ) (b) and the loss function (c) of $HoMnO_3$ single crystals for $\vec{E} \perp z$ (a) at $T = 300$ K.

in $HoMnO_3$ below 300 K. One of the Raman-active E_2-symmetry phonons, however, is strongly affected by the antiferromagnetic ordering of Mn ions *within* the xy plane below T_N. As seen from the inset in figure 4, its frequency deviates from the dependence expected for anharmonic decay and hardens by as much as 5 cm^{-1} between T_N and 10 K. The vibrational pattern of this eigenmode (calculated at 231 cm^{-1}) is displayed in figure 5(a). The mode involves displacements of Mn, O2 and O3 ions in the xy plane. It could be viewed as asymmetric deformations of Mn_3O_3 'rings' (as Mn and O ions move in anti-phase) along with the in-plane 'rotations' of the neighbouring Mn_3O_3 structural units. This mode effectively modulates Mn–O–Mn bond angles and, hence, the Mn–Mn exchange interaction. Similar phonon frequency anomalies near the magnetic ordering temperature have been reported earlier for CuO [16], $SrRuO_3$ [17] and CrO_2 [18, 19].

Another unusual feature of the temperature-dependent Raman spectra of $HoMnO_3$ is the monotonic intensity increase (by a factor of about three) upon cooling from 300 to 10 K of the A_1-symmetry line at 685 cm^{-1} in the (xx) scattering configuration. It may, at least in part, be due to the temperature-induced shift by about 0.19 eV toward higher energies of the on-side Mn d–d transition [13], which changes the resonant conditions.

The spectral dependence of the imaginary part of the $HoMnO_3$ dielectric function is shown in figure 6 for several temperatures between 300 and 10 K. Here, similar to the E_2 symmetry mode discussed above, one of the modes, centred at 230 cm^{-1} at room temperature, exhibits

Table 1. Calculated and experimentally observed at 300 K Raman spectra A_1 and E_2 symmetry Γ-point phonon frequencies of hexagonal $HoMnO_3$ (in cm^{-1}).

Mode	Theory (TO/LO)	Experiment Raman (TO/LO)	Direction of the largest atomic displacements
A_1	125/127		z(Ho)
A_1	195/234		$rot_{xy}(MnO_5)$
A_1	245/270	262/262	$+z$(Ho) $-$ z(Mn)
A_1	291/295	295/295	x(Mn), z(O3)
A_1	404/428	411/—	$+z$(O3, O4) + x, y(O2) $-$ x, y(O1)
A_1	430/460	427/427	$+z$(O4, O3) $-$ z(Mn)
A_1	468/474	463/463	$+x$, y(O1, O2) $-$ x, y(Mn)
A_1	598/614		$+z$(O1, O2) $-$ z(Mn)
A_1	673/673	685/685	$+z$(O1) $-$ z(O2)
E_2	64		x, y(Ho, Mn)
E_2	96		$+x$, y(Mn, O3, O4) $-$ x, y(Ho)
E_2	137	136	x, y(Ho)
E_2	152		x, y(Ho)
E_2	231	221	$+x$, y(Mn) $-$ x, y(O3, O4)
E_2	254		z(Mn, O2, O1)
E_2	265		z(Mn, O1, O2)
E_2	330	295	z(O2, O1), x, y(O4)
E_2	339		$+x$, y(O1, O2, O4, O3) $-$ x, y(Mn)
E_2	402		$+x$, y(O1, O4) $-$ x, y(O2, Mn)
E_2	468	442	$+x$, y(O4) $-$ x, y(O1, Mn)
E_2	523		x, y(O4, O3, O1, O2)
E_2	557		x, y(O4)
E_2	583		x, y(O4, O3)
E_2	649		x, y(O3, O4)

Table 2. Calculated and experimentally observed at 300 K E_1 symmetry Γ-point phonon frequencies of hexagonal $HoMnO_3$ (in cm^{-1}).

Mode	Theory TO/LO	Experiment IR (TO/LO)	Experiment Raman (TO)	Direction of the largest atomic displacements
E_1	107/110			$+x$, y(Mn, O3, O4) $-$ x, y(Ho)
E_1	143/143	136/146		x, y(Ho)
E_1	149/149	160/164		x, y(Ho)
E_1	231/231			$+x$, y(O1, O2) $-$ x, y(Ho)
E_1	247/253	230/278		x, y(O3, O4) + x, z(O1, O2); z(Mn)
E_1	262/336	289/301		$+x$, y(O1, O2) $-$ x, y(O3)
E_1	337/358	303/326		$+x$, y(O1, O2, O3) $-$ x, y(O4, Mn)
E_1	359/397	355/357	354	$+x$, y(O1) $-$ x, y(O2)
E_1	398/410	369/410	369	$+x$, y(O1) $-$ x, y(O2)
E_1	471/491	418/476	419	$+x$, y(O4, O3) $-$ x, y(O2, O1, Mn)
E_1	497/537	479/551	480	$+x$, y(O4, O3, O1, O2) $-$ x, y(Mn)
E_1	568/571			x, y(O4)
E_1	585/586	593/601		x, y(O3)
E_1	648/648		636	x, y(O3) $-$ x, y(O4)

remarkable frequency hardening upon entering the antiferromagnetic state. According to the lattice dynamics calculations (figure 5(b)) this E_1 symmetry mode is of a more complex shape compared to the E_2 mode depicted in figure 5(a) and corresponds to in-xy-plane displacements

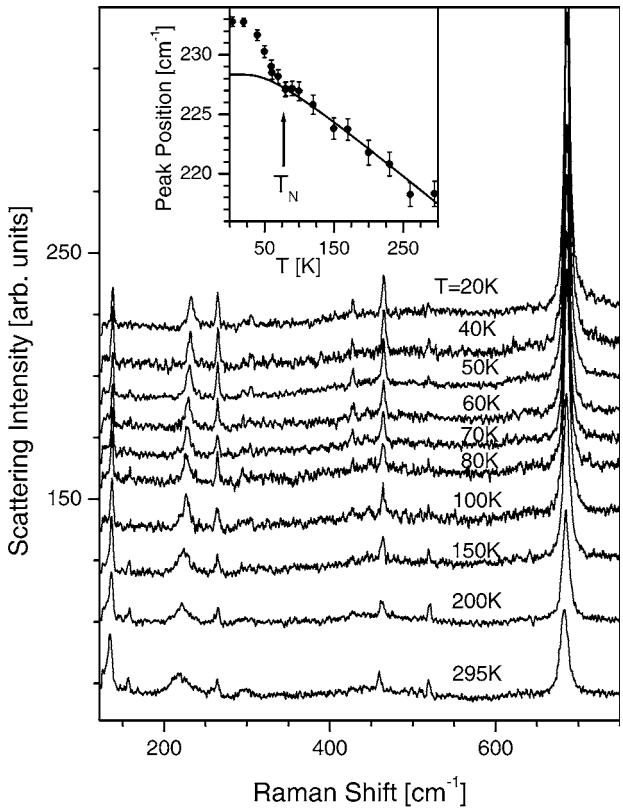

Figure 4. Raman scattering spectra of $HoMnO_3$ in $z(xx)\bar{z}$ polarization for various temperatures between 20 and 295 K ($\lambda_{exc} = 514.5$ nm). The inset displays the position of one of the E_2 symmetry modes versus temperature. The full curve shows the peak position expected for a standard anharmonicity-related phonon decay. T_N marks the Néel temperature.

Table 3. Shell model parameters for $HoMnO_3$.

Ion	Z (|e|)	Y (|e|)	α (Å^3)	Ionic pair	a (eV)	b (Å^{-1})	c (eV Å^6)
Ho	2.85	1.7	0.7	Ho–O	1 738	3.04	0
Mn	2.85	3.0	3.0	Mn–O	2 020	3.35	0
O	−1.90	−3.0	2.0	O–O	22 764	6.710	20.37

of the basal O3 and O4 ions in phase with the motion of the apical O1 and O2 ions (the latter do also have an out-of-plane component). As Mn ions move only in the z direction, the deformation of Mn–O–Mn angles is obvious. Thus, in close similarity to the E_2 vibration discussed above, the E_1 mode modulates the in-xy-plane Mn–O–Mn bonds. It is worth noting that an unusual temperature behaviour of low frequency phonon E_1 modes was recently observed in the infrared reflection spectra of isostructural hexagonal $LuMnO_3$ single crystals, suggesting their coupling to the spin system [14].

Several very narrow lines (with full width at half-maximum as low as 3 cm^{-1}), which become especially pronounced at lower temperatures at around 160 and 240 cm^{-1}, are related to the intramultiplet transitions of the Ho^{3+} ground multiplet, split by the crystal field. These transitions, as well as those between ground ($^5I_8$) and excited ($^5I_7$ and $^5I_6$) states, will be discussed in detail elsewhere [13].

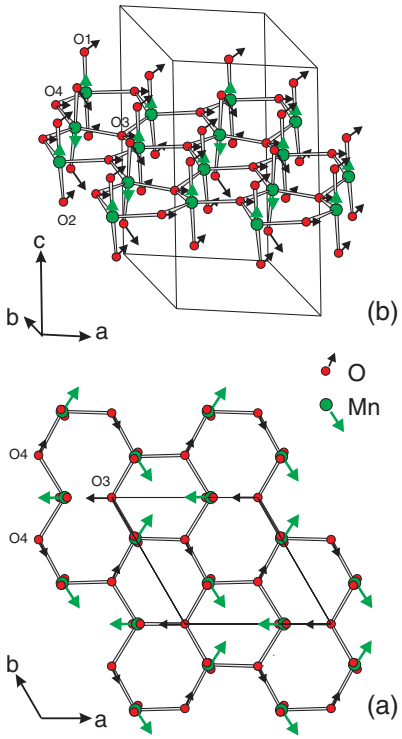

Figure 5. Calculated within a shell model are ion displacements for two vibrational modes, which exhibit pronounced anomalies in the antiferromagnetic phase below T_N: E_2-symmetry mode at 231 cm^{-1} (a) and E_1(TO)-mode at 247 cm^{-1} (b).

(This figure is in colour only in the electronic version)

3.3. Second-order Raman scattering spectra

Unlike the first-order scattering which, due to momentum conservation, probes only zone-centre (Γ-point) vibrations, the second order scattering involves phonons throughout the entire Brillouin zone. The scattering intensity in this case is governed by both the scattering selection rules and also the phonon density of state, which is determined by the phonon dispersion.

The second-order scattering spectra of $HoMnO_3$ single crystals in various scattering configurations at temperatures 300 and 10 K are displayed in figure 7. No second-order bands are detected in the spectra obtained for (xy) and (xz) polarizations (the two lowest curves in figure 7), while several bands appear in the (xx) and (zz) polarized spectra, which probe the A_1 symmetry excitations. It is known that for the hexagonal space groups, including $P6_3cm$ (C^3_{6v}), the overtones for all special points of the Brillouin zone always contribute to the fully symmetric A_1 component, while combinations of phonons belonging to different symmetries never contain a A_1 representation (see, e.g., [20, 21]).

The cut-off frequency of the two-phonon spectrum is expected to be at the double frequency of the highest energy Γ-point phonon ($2 \times 685\ cm^{-1} = 1370\ cm^{-1}$). The peak at 1368 cm^{-1}, which is observed in the (xx) polarization, corresponds to the overtone of the highest frequency A_1-symmetry phonon at the Brillouin zone centre. The peak at the lower frequency, 1280 cm^{-1}, which is observed in both (xx) and (zz) scattering geometries, is due to the overtone of the same vibration at the zone-boundary point K, situated along the x axis (see, for example, [22]

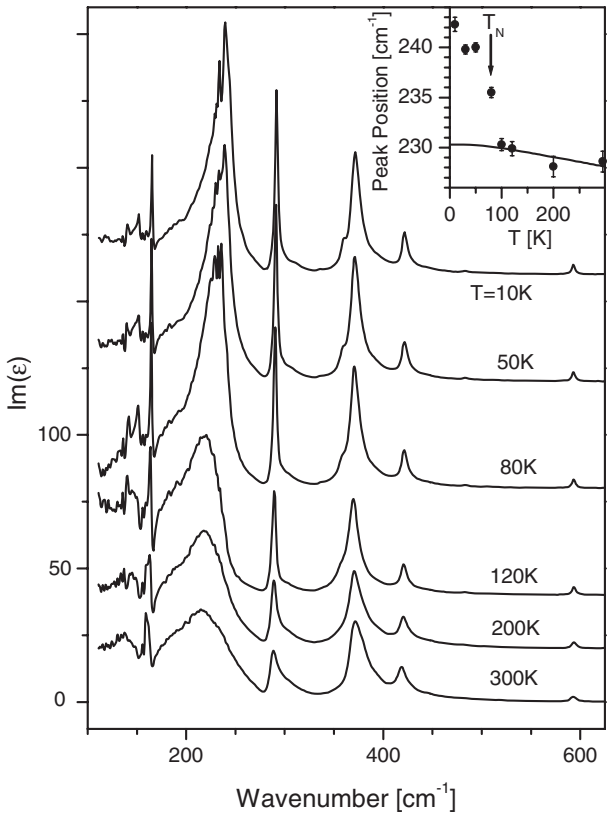

Figure 6. Temperature dependence of $\mathrm{Im}(\epsilon)$ for $HoMnO_3$ single crystals ($\vec{E} \perp z$). The spectra are displaced vertically for clarity. The inset shows the peak position of a low-frequency mode, which exhibits anomalous hardening below the Néel temperature T_N. The full curve is the behaviour expected for a standard anharmonicity-related shift.

for special points notation). Indeed, our shell-model calculations predict softening of the high-frequency optical vibrations by 35 cm^{-1} along the x axis, but only by a few wavenumbers along the z axis (at the A point of the Brillouin zone). Thus, the experimental data reveal that the dispersion of the high-frequency branch through the Brillouin zone in the x direction is approximately 45 cm^{-1}.

Several peaks in the frequency range 1080–1117, which are especially pronounced in the (xx) polarization at 10 K, are probably due to combinations of the high-frequency mode with the phonon branches in the range 350–463 cm^{-1} at various points of the Brillouin zone. The broad peak centred at 874 cm^{-1} is likely related to the overtones of these latter modes. We note that the second-order Raman scattering spectra for hexagonal $HoMnO_3$ are very similar to those reported earlier for $YMnO_3$ in terms of relative line intensities and position of the most intense features [10].

4. Conclusions

The phonon excitations in hexagonal $HoMnO_3$ single crystals are studied by means of polarized Raman scattering and infrared reflection spectroscopy. The zone-centre vibrations are assigned

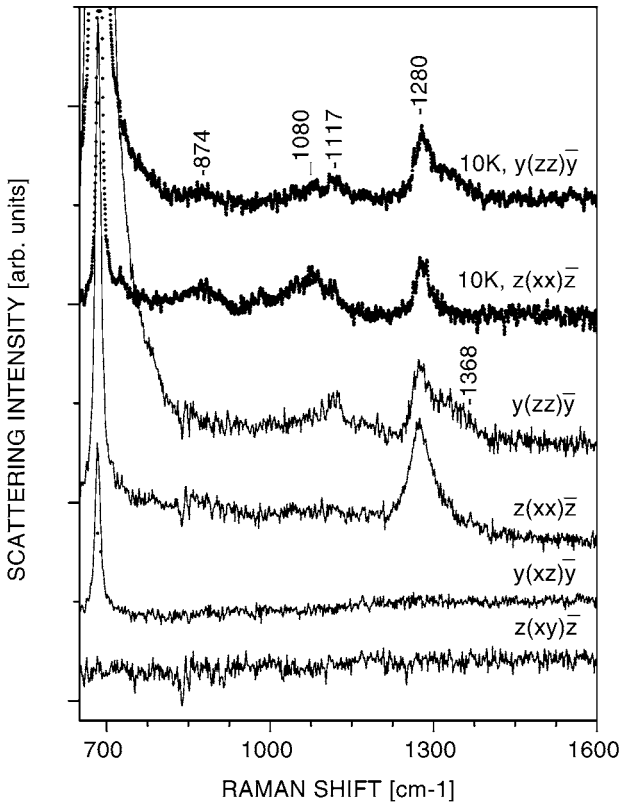

Figure 7. Second-order polarized Raman scattering spectra of $HoMnO_3$ for $\lambda_{exc} = 514.5$ nm. Two upper spectra are taken at $T = 10$ K, and the lower four at 300 K.

to definite modes based on their polarization properties and the results of lattice dynamics calculations. In agreement with calculations, the second-order Raman scattering data allow us to conclude that the dispersion of the high frequency optical modes is about 45 cm^{-1} along the x direction in the Brillouin zone. Two phonon modes, which modulate the Mn–Mn interaction, exhibit pronounced anomalies near the magnetic ordering temperature $T_N = 76$ K, a fact that provides experimental evidence for a relatively strong spin–phonon coupling in $HoMnO_3$.

Acknowledgments

This work is supported in part by the State of Texas through the Texas Center for Superconductivity and Advanced Materials at the University of Houston. MMG greatly acknowledges the support of the Bulgarian Science Found (Project F-1207).

References

[1] Smolenskii G A and Chupis I E 1982 *Usp. Fiz. Nauk* **136–138** 415
Smolenskii G A and Chupis I E 1982 *Sov. Phys.—Usp.* **25** 475
[2] Kimura T, Goto T, Shintani H, Ishizaka K, Arima T and Tokura Y 2003 *Nature* **426** 55
[3] Huang Z J, Cao Y, Sun Y Y, Xue Y Y and Chu C W 1997 *Phys. Rev.* B **56** 2623
[4] Fröhlich D, Leute S, Pavlov V V and Pisarev R V 1998 *Phys. Rev. Lett.* **81** 3239

[5] Iizuka-Sakano T, Hanamura E and Tanabe Y 2001 *J. Phys.: Condens. Matter* **13** 3031
[6] Fiebig M, Lottermoser Th, Fröhlich D, Goltsev A V and Pisarev R V 2002 *Nature* **419** 818
[7] Fiebig M, Fröhlich D, Kohn K, Leute St, Lottermoser Th, Pavlov V V and Pisarev R V 2000 *Phys. Rev. Lett.* **84** 5620
[8] Muños A, Alonso J A, Martínez-Lope M J, Casáis M T, Martínez J L and Fernández-Diaz M T 2001 *Chem. Mater.* **13** 1497
[9] Takahashi J, Hagita K, Kohn K, Tanabe Y and Hanamura E 2002 *Phys. Rev. Lett.* **89** 076404
[10] Iliev M N, Hadjiev V G, Litvinchuk A P and Meng R L 2003 *Phys. Rev. Lett.* **90** 069701
[11] Sato T J, Lee S-H, Katsufuji T, Masaki M, Park S, Copley J R D and Takagi H 2003 *Phys. Rev.* B **68** 014432
[12] Iliev M N, Lee H-G, Popov V N, Abrashev M V, Hamed A, Meng R L and Chu C W 1997 *Phys. Rev.* B **56** 2488
[13] Litvinchuk A P *et al* unpublished results
[14] Souchkov A B, Simpson J R, Quijada M, Ishibashi H, Hur N, Ahn J S, Cheong S W, Millis A J and Drew H D 2003 *Phys. Rev. Lett.* **91** 027203
[15] Popov V N 1995 *J. Phys.: Condens. Matter* **7** 1625
[16] Chen X K, Irwin J C and Frank J P 1995 *Phys. Rev.* B **52** R13130
[17] Iliev M N, Litvinchuk A P, Lee H-G, Chen C L, Dezaneti M L and Chu C W 1999 *Phys. Rev.* B **59** 364
[18] Iliev M N, Litvinchuk A P, Lee H-G, Chu C W, Barry A and Coey J M D 1999 *Phys. Rev.* B **60** 33
[19] Yu T, Shen Z X, Sun W X, Lin J Y and Ding J 2003 *J. Phys.: Condens. Matter* **15** L213
[20] Gorban' I S and Lugovoi V I 1976 *Zh. Prikl. Spektrosk.* **24** 333
Gorban' I S and Lugovoi V I 1976 *J. Appl. Spectrosc.* **24** 233
[21] Siegle H, Kaczmarczyk G, Filippidis L, Litvinchuk A P, Hoffmann A and Thomsen C 1997 *Phys. Rev.* B **55** 7000
[22] Burns G and Glazer A M 1993 *Space Groups for Solid State Scientists* (New York: Academic)